Inorg. Chem. **2005**, *44*, 4333–4345

Synthesis, Structure, and Electrochemical Properties of Copper(I) Complexes with S/N Homoscorpionate and Heteroscorpionate Ligands

Roberto Cammi, Marcello Gennari, Marco Giannetto, Maurizio Lanfranchi, Luciano Marchiò,* Giovanni Mori, Cristiano Paiola, and Maria Angela Pellinghelli

Dipartimento di Chimica Generale ed Inorganica, Chimica Analitica, Chimica Fisica, Parco area delle Scienze 17a, 43100 Parma, Italy

Received December 17, 2004

Dinuclear Cu(I) complexes with bifunctionalized homoscorpionate ligands, hydrotris(thioxotriazolyl)borato [Li($Tr^{Me,o-Py}$) (**1**) and Li($Tr^{Mes,Me}$) (**2**)], and the heteroscorpionate ligand hydro[bis(thioxotriazolyl)-3-(2-pyridyl)pyrazolyl]borato [K($Br^{Mes}pz^{o-Py}$)] (**3**) were synthesized and crystallographically characterized. The complexes $[Cu(Tr^{Mes,Me})]_2$ (**4**) and $[Cu(Tr^{Me,o-Py})]_2$ (**5**) exhibit a similar coordination geometry where every metal is surrounded by three thioxo groups in a trigonal arrangement. The presence of a [B–H···Cu] three-center–two-electron interaction in both compounds causes the overall coordination to become tetrahedrally distorted (S_3H coordination for each metal). The complex $[Cu(Br^{Mes}pz^{o-Py})]_2$ (**6**) presents a trigonal geometry in which the metals interact with two thioxo groups and a bridging pyrazolyl nitrogen atom. A weak contact with a pyridine nitrogen atom completes the coordination of the metals (S_2N,N' coordination for each metal). $[Cu(Tr^{Mes,Me})]_2$, $[Cu(Tr^{Me,o-Py})]_2$, and $[Cu(Br^{Mes}pz^{o-Py})]_2$ exhibit fluxional behavior in solution as evidenced by variable-temperature NMR spectroscopy, and for **5** and **6** two species in equilibrium [in the ratio 2/1 for **5** ($CDCl_3$) and 3/2 for **6** (CD_2Cl_2)] are distinguishable in the ^1H NMR spectra at 270 K. 2D-NOESY spectra recorded at 270 K assisted in the attribution of solution molecular geometries for each isomer of **5** and **6**. The free energy of activation ($\Delta G^{\ddagger}_{Tc}$) was determined for both equilibria from the evaluation of the coalescence temperature. DFT calculations were performed to describe plausible molecular geometry for the minor isomer of **5** and **6** and to propose a possible mechanism of interconversion between major and minor isomers. Cyclic voltammograms were recorded in CH_2Cl_2 (**3** and **6**) or CH_2Cl_2/CH_3CN (1/1, v/v) (**2**, **4**, and **5**) solutions using 0.1 M TBAHFP or TBAOTf as supporting electrolytes. $[Cu(Tr^{Mes,Me})]_2$, $[Cu(Tr^{Me,o-Py})]_2$, and $[Cu(Br^{Mes}pz^{o-Py})]_2$ exhibit a quasi-reversible Cu(I)/Cu(II) redox behavior with $E_{pa} = +719$ mV and $E_{pc} = +538$ mV for **4**, $E_{pa} = +636$ mV and $E_{pc} = -316$ mV for **5**, and $E_{pa} = +418$ mV and $E_{pc} = -319$ mV for **6**.

Introduction

Cupredoxins are small copper proteins (10−20 kDa) soluble in water, which control electron flow from donor to acceptor biomolecules in respiratory and photosynthetic processes of many bacteria and plants.[1−4] In the natural state they contain intensely colored Cu(II)−thiolate sites and are classified in three types,[5] according to the metal coordination: type 1 (T1); type 2 (T2); type Cu_A. The unusual coordination of T1 centers, intermediate between trigonal and distorted tetrahedral, is characterized by strong bonds between the metal and three donor atoms on a plane (N−His, N−His, S−Cys) and by a weaker interaction with a fourth axial ligand (usually S-Met). T1 sites are subdivided in *T1 trigonal* (typical of blue copper proteins, such as plastocyanin,[6] azurin,[7] and ceruloplasmin[8]) and *T1 distorted*

* Author to whom correspondence should be addressed. E-mail: marchio@unipr.it.

(1) Adman, E. T. *Adv. Protein Chem.* **1991**, *42*, 145−197.
(2) Beinert, H. *J. Inorg. Biochem.* **1996**, *64*, 79−135.
(3) Gray, H. B.; Malmstrom, B. G.; Williams, R. J. P. *J. Biol. Inorg. Chem.* **2000**, *5*, 551−559.
(4) Solomon, E. I.; Baldwin, M. J.; Lowery, M. D. *Chem. Rev.* **1992**, *92*, 521−542.
(5) Holm, R. H.; Kennepohl, P.; Solomon, E. I. *Chem. Rev.* **1996**, *96*, 2239−2314.
(6) (a) Colman, P. M.; Freeman, H. C.; Guss, J. M.; Murata, M.; Norris, V. A.; Ramshaw, J. A. M.; Venktappa, M. P. *Nature* **1978**, *272*, 319−324. (b) Shibata, N.; Inoue, T.; Nagano, C.; Nishio, N.; Kohzuma, T.; Onodera, K.; Yoshizaki, F.; Sugimura, Y.; Kai, Y. *J. Biol. Chem.* **1999**, *274*, 4225−4230.
(7) Adman, E. T.; Stenkamp, R. E.; Sieker, L. C.; Jensen, L. H. *J. Mol. Biol.* **1978**, *123*, 35−45.
(8) Zaitseva, I.; Zaitsev, V.; Card, G.; Moshkov, K.; Bax, B.; Ralph, A.; Lindley, P. *J. Biol. Inorg. Chem.* **1996**, *1*, 15−23.

10.1021/ic048221j CCC: $30.25
Published on Web 05/12/2005

Chart 1

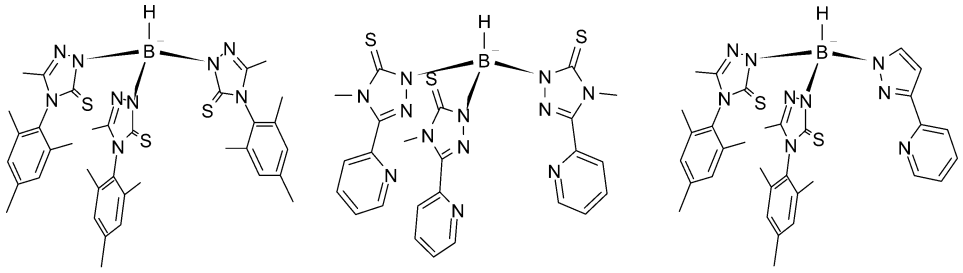

tetrahedral (blue nitrite reductasi[9]), depending on the effective geometry of the metal. Copper geometry and donor atom sets have important consequences on the function of these proteins. According to the entatic state theory,[10] the metal coordination geometry is imposed by the protein matrix, which forces the Cu(II) site to adopt a geometry similar to that needed for requirements of Cu(I). This would favor a reversible and fast electron transfer since it is associated with low reorganization energy during the redox process.[11] Other authors have questioned the entatic-state theory and suggest that the metal geometry is mainly dictated by the coordination environment and donor set [S(thiolate), S(thioether), N(imidazole)] instead of being determined by the protein framework.[12−15]

Several Cu(II) and Cu(I) complexes, which model T1 sites of cupredoxins, are reported in the literature. Some of these models are represented by dinuclear Cu(I) complexes with hydrotris(pyrazolyl)borato ligands ($Tp^{RR'}$) where the metal exhibits a trigonal geometry[16] whereas other systems achieve a tetrahedral copper coordination by means of a facially bound Tp ligand and additional monodentate donor groups.[17−19] N_2S_2 donor ligands based on the biphenyl platform[20] have been especially designed to provide a rigid and tetrahedral ligand framework around Cu(II) to meet the requirements of the entatic-state theory. Other systems are based on the bis(benzimidazoles)−thioether ligands which are able to give a wide variety of metal coordination spanning from the planar trigonal to the trigonal bipyramidal.[21,22] Recently, bulky β-diketiminate ligands associated with a thiolate group have been able to reproduce the unusual trigonal geometry at Cu(II) occurring in type I centers.[23] In these low molecular weight complexes the ligand topology, the donor set, and the metal coordination geometry imposed by the ligands modulate the redox activity of the Cu(II)/Cu(I) couple.

This work regards the synthesis of Cu(I) complexes with the homoscorpionate hydrotris(thioxotriazolyl)borato [$(Tr^{Me,o-Py})^-$ and $(Tr^{Mes,Me})^-$] ligands and the heteroscorpionate[24] hydro[bis(thioxotriazolyl)-3-(2-pyridyl)pyrazolyl]borato [$(Br^{Mes}pz^{o-Py})^-$] ligand (Chart 1) aimed at obtaining models for T1 sites. Even though these ligands may adopt rather different modes of coordination by virtue of the different substituents on the triazoline rings, the dinuclear Cu(I) complexes exhibit quite similar solid-state structures with respect to the metal geometry. In fact, the metals adopt a trigonal geometry, which is distorted toward the tetrahedral one by a [B−H···Cu] interaction for $[Cu(Tr^{Mes,Me})]_2$ and $[Cu(Tr^{Me,o-Py})]_2$ and by a Cu···$N_{pyridine}$ interaction for $[Cu(Br^{Mes}pz^{o-Py})]_2$. Many examples of dinuclear Cu(I) complexes with Tp ligands have been reported where the metal adopts a linear or trigonal[16,25] coordination according to the steric constraints determined by bulky substituents placed on different parts of the ligands. The high flexibility of $(Tr^{Me,o-Py})^-$, $(Tr^{Mes,Me})^-$, and $(Br^{Mes}pz^{o-Py})^-$ may limit the influence of the steric hindrance on the metal geometry. As a consequence, it is possible to infer that the resulting coordination environments are mainly dictated by the metal requirements and only to a less extent by ligand constraints.

(9) Inoue, T.; Gotowda, M.; Deligeer; Kataoka, K.; Yamaguchi, K.; Suzuki, S.; Watanabe, H.; Goho, M.; Kai, Y. *J. Biochem. (Tokyo)* **1998**, *124*, 876−879.

(10) (a) Vellee, B. L.; Williams, R. J. P. *Proc. Natl. Acad. Sci. U.S.A.* **1968**, *59*, 498−505. (b) Williams, R. J. P. *Eur. J. Biochem.* **1995**, *234*, 363−381.

(11) Marcus, R. A.; Sutin, N. W. *Biochim. Biophys. Acta* **1985**, *811*, 265−322.

(12) Messerschmidt, A.; Prade, L.; Kroes, S. J.; Sanders-Loehr, J.; Huber, R.; Canters, G. W. *Proc. Natl. Acad. Sci. U.S.A.* **1998**, *95*, 3443−3448.

(13) (a) Ryde, U.; Olsson, M. H. M.; Pierloot, K.; Roos, B. O. *J. Mol. Biol.* **1996**, *261*, 586−596. (b) Ryde, U.; Olsson, M. H. M.; Roos, B. O.; Borin, A. C. *Theor. Chem. Acc.* **2001**, *105*, 452−462.

(14) Ryde, U.; Olsson, M. H. M.; Pierloot, K. *Theor. Comput. Chem.* **2001**, *9*, 1−55.

(15) Guckert, J. A.; Lowery, M. D.; Solomon, E. I. *J. Am. Chem. Soc.* **1995**, *117*, 2817−2844.

(16) Carrier, S. M.; Ruggiero, C. E.; Houser, R. P.; Tolman, W. B. *Inorg. Chem.* **1993**, *32*, 4889−4899.

(17) Randall, D. W.; George, S. D.; Hedman, B.; Hodgson, K. O.; Fujisawa, K.; Solomon, E. I. *J. Am. Chem. Soc.* **2000**, *122*, 11620−11631.

(18) Kitajima, N.; Fujisawa, K.; Moro-oka, Y. *J. Am. Chem. Soc.* **1990**, *112*, 3210−3212.

(19) Kitajima, N.; Fujisawa, K.; Tanaka, M.; Moro-oka, Y. *J. Am. Chem Soc.* **1992**, *114*, 9232−9233.

(20) Malachowski, M. R.; Adams, M.; Elia, N.; Rheingold, A. L.; Kelly, R. S. *J. Chem. Soc., Dalton Trans.* **1999**, 2177−2182.

(21) Balamurugan, R.; Palaniandavar, M. *Inorg. Chem.* **2001**, *40*, 2246−2255.

(22) Vaidyanathan, M.; Balamurugan, R.; Sivagnanam, U.; Palaniandavar, M. *J. Chem. Soc., Dalton Trans.* **2001**, 3498−3506.

(23) (a) Holland, P. L.; Tolman, W. B. *J. Am. Chem. Soc.* **1999**, *121*, 7270−7271. (b) Randall, D. W.; DeBeer George, S.; Holland, P. L.; Hedman, B.; Hodgson, K. O.; Tolman, W. B.; Solomon, E. I. *J. Am. Chem. Soc.* **2000**, *122*, 11632−11648.

(24) The definition homoscorpionate and heteroscorpionate have been adopted in analogy to the poly(pyrazolyl)borate nomenclature: Trofimenko, S. *Chem. Rev.* **1993**, *93*, 943−980.

(25) (a) Yoon, K.; Parkin, G. *Polyhedron* **1995**, *14*, 811−821. (b) Kiani, S.; Long, J. R.; Stavropoulos, P. *Inorg. Chim. Acta* **1997**, *263*, 357−366. (c) Mealli, C.; Arcus, C. S.; Wilkinson, J. L.; Marks, T. J.; Ibers, J. A. *J. Am. Chem. Soc.* **1976**, *98*, 711−718. (d) Carrier, S. M.; Ruggiero, C. E.; Tolman, W. B. *J. Am. Chem. Soc.* **1992**, *114*, 4407−4408.

By means of cyclic voltammetry the main electrochemical parameters of the redox couple Cu(I)/Cu(II) have been evaluated for the complexes, and they are discussed in relation to solid state and solution structural properties, obtained by X-ray diffration and variable-temperature and 2D NMR spectroscopy, respectively.

Experimental Section

General Procedures. All reagents were purchased from Sigma-Aldrich except mesityl isothiocyanate,[26] 3-(2-pyridyl)pyrazole,[27] $LiTr^{Me,o-Py}$ (**1**),[28] and $[Cu(CH_3CN)_4]BF_4$,[29] which were prepared using methods reported in the literature. All solvents were commercially available and were used without further purification except THF and toluene, which were distilled on sodium−benzophenone and sodium, respectively, and stored under nitrogen. Acetonitrile and methanol were stored on molecular sieves 4 Å (1−2 mm) and degassed prior to use. Syntheses of tripodal ligands and complexes were performed in inert gas (N_2) using Schlenk techniques. CI-MS spectra were recorded on a Finnigan 1020 mass spectrometer in positive-ion mode with a quadrupole MATTSSQ 710. ESI-MS spectra were recorded on a Micromass ZMD spectrometer. The solutions were analyzed in both positive and negative ionization mode. Infrared spectra were recorded as KBr pellets from 4000 to 400 cm^{-1} on a Perkin-Elmer FT-IR Nexus. Elemental analyses were performed on a Carlo Erba EA 1108 automatic analyzer.

Preparation of 4-Mesityl-3-methyl-5-thioxotriazole. Mesityl isothiocyanate (4.8 g, 27 mmol) and acetic hydrazide (2.2 g, 27 mmol) were dissolved in absolute ethanol (35 mL). The solution was heated to reflux and stirred. After about 2.5 h a white solid precipitated. Heating was stopped after 4.5 h, and the solid was filtered off and washed with absolute ethanol (20 mL). It was then dissolved in aqueous NaOH (2 M, 90 mL) and refluxed for 7 h. The white suspension was filtered, and the solution was treated with HCl (at first 10 M and then 3 M) until neutral pH. The white solid that formed was filtered off, washed with H_2O, vacuum-dried, and collected (4.8 g, 21 mmol, 78%). IR (KBr pellet, cm^{-1}): 3116 s, 3062 m, 2941 s, 1584 w, 1496 m, 1328 s. ^1H NMR (300 MHz, 298 K, $CDCl_3$): δ 2.07 (s, 6H, CH_3), 2.11 (s, 3H, CH_3), 2.37 (s, 3H, CH_3), 7.06 (s, 2H, CH Mes), 11.95 (bs, 1H, NH). MS (CI, *m*/*z*, I %): 233, 50 [M^+]; 234, 100 [MH^+]. Anal. Calcd for $C_{12}H_{15}N_3S$ (M_r = 233.33): C, 61.77; H 6.48; N, 18.01. Found: C, 61.49; H, 6.48; N, 17.67.

Preparation of $LiTr^{Mes,Me}$ (2). 4-Mesityl-3-methyl-5-thioxotriazole (4.000 g, 17.14 mmol), $LiBH_4$ (0.125 g, 5.45 mmol), and toluene (80 mL) were mixed together in a Schlenk flask connected to a water condenser and to an oil-bubbler. During stirring, the temperature was increased to 135 °C. After some hours a white solid began to precipitate. After 3 days, the hot mixture was filtered and the solid washed with hot toluene (3 × 20 mL), vacuum-dried, and collected (3.7 g, 5.2 mmol, 95%). IR (KBr pellet, cm^{-1}): 3010 w, 2920 m, 2854 w, 2550 w [ν(BH)], 1610 m, 1583 m, 1490 s, 1410 vs, 1323 s, 1136 m, 1015 m. ^1H NMR (300 MHz, 298 K, DMSO-d_6): δ 1.85 (m, 9H, CH_3), 1.96 (m, 18H, CH_3), 2.30 (s, 9H, CH_3), 4.93 (s br, 1H, BH), 7.00 (m, 6H, CH Mes). ^{13}C NMR (75 MHz, 298 K, DMSO-d_6): δ 11.26 (CH_3), 17.49 (CH_3), 20.65 (CH_3), 128.65 (CH Mes), 131.13 (C quat), 136.06 (C quat), 137.87 (C quat), 145.13 (C quat), 168.95 (C═S). MS (CI, *m*/*z*, I %): 233, 100; 715, 6 [M^+]. Anal. Calcd for $C_{36}H_{43}N_9S_3BLi$ (M_r = 715.74): C, 60.41; H, 6.05; N, 17.61. Found: C 59.89; H 5.96; N 17.31.

Preparation of $KBr^{Mes,Me}pz^{o-Py}$ (3). 4-Mesityl-3-methyl-5-thioxotriazole (1.00 g, 4.28 mmol), 3-(2-pyridyl)pyrazole (0.351 g, 2.42 mmol), KBH_4 (0.119 g, 2.21 mmol), and toluene (50 mL) were added to a Schlenk flask connected to a water condenser and to an oil-bubbler. While the solution was being stirred, the temperature was raised to 150 °C. A white precipitate formed after 1 night. The mixture was allowed to react for 9 days. It was then filtered, and the solid was washed with hot toluene (20 mL) and with a 2/1 dichloromethane/ethanol mixture (30 mL), vacuum-dried, and collected (0.797 g, 1.21 mmol, 56%). IR (KBr pellet, cm^{-1}): 3018 w, 2920 m, 2854 w, 2441 w [ν(BH)], 1595 m, 1491 m, 1429 m, 1409 s, 1382 m, 1359 s, 1323 m, 1299 m, 1265 m, 1205 m. ^1H NMR (300 MHz, 298 K, DMSO-d_6): δ 1.84 (s, 6H, CH_3), 1.93 (s, 6H, CH_3), 1.95 (s, 6H, CH_3), 2.29 (s, 6H, CH_3), 4.92 (s br, 1H, BH), 6.67 (d, J = 2 Hz, 1H, CH pz), 7.00 (s, 4H, Mes), 7.20 (m, 1H, CH py), 7.59 (d, J = 2 Hz, 1H, CH pz), 7.76 (t, J = 7.8 Hz, 1H, CH py), 7.98 (d, J = 7.8 Hz, 1H, CH py), 8.52 (d, J = 4.5 Hz, 1H, CH py). ^{13}C NMR (75 MHz, 298 K, DMSO-d_6): δ 11.07 (CH_3), 17.34 (CH_3), 17.44 (CH_3), 20.59 (CH_3), 102.15 (CH pz), 118.85 (CH py), 121.09 (CH py), 128.61 (CH Mes), 128.73 (CH Mes), 130.89 (C quat), 134.65 (C quat), 135.77 (CH pz), 136.07 (CH py), 137.98 (C quat), 145.64 (C quat), 148.79 (CH py), 154.06 (C quat), 168.75 (C═S). ESI-MS (cone 26 V, negative ion mode, 1/1 CH_3CN/MeOH, *m*/*z*, I %): 620.1, 100 [L] [L = $(Br^{Mes,Me}pz^{o-Py})^-$]. Anal. Calcd for $C_{32}H_{35}N_9S_2BK$ (M_r = 659.72): C, 60.41; H, 5.35; N, 17.61. Found: C, 59.95; H, 5.61; N 17.70.

Preparation of $[Cu(Tr^{Mes,Me})]_2$ (4). A solution of $Cu(MeCN)_4BF_4$ (0.132 g, 0.419 mmol) in methanol (3 mL) was added to a stirred mixture of $LiTr^{Mes,Me}$ (0.300 g, 0.419 mmol) in methanol (20 mL). The suspension became dark immediately, and it cleared after a few minutes giving a white precipitate. After 2 h the solid was filtered off, washed with methanol (5 mL), vacuum-dried, and collected (0.117 g, 0.076 mmol, 36%). IR (KBr pellet, cm^{-1}): 3009 w, 2966 w, 2949 w, 2920 m, 2857 w, 2491 w [ν(BH)], 1609 w, 1576 w, 1488 m, 1407 s, 1371 m, 1328 s, 1302 m. ^1H NMR (300 MHz, 298 K, $CDCl_3$): δ 1.93 (s, 36H, CH_3), 1.98 (s, 18H, CH_3), 2.29 (s, 18H, CH_3), 6.90 (s, 12H, CH Mes). ^{13}C NMR (75 MHz, 298 K, $CDCl_3$): δ 11.20 (*o*-CH_3 Mes), 17.88 (*p*-CH_3 Mes), 21.06 (CH_3 triazoline), 128.97 (CH Mes), 130.17 (C quat), 136.30 (C quat), 138.97 (C quat), 147.62 (C quat), 167.80 (C═S). ESI-MS (cone 50 V, positive ion mode, 1/1 CH_3CN/MeOH, *m*/*z*, I %): 3127.8, 10 $[CuL]_4K^+$; 2380.1, 12 $[Cu_4L_3]^+$; 2355.2, 32 $[CuL]_3K^+$; 2339.5, 13 $[CuL]_3Na^+$; 1607.7, 68 $[Cu_3L_2]^+$; 1583.3, 85 $[CuL]_2K^+$; 1567.2, 43, $[CuL]_2Na^+$; 834.7, 7 $[Cu_2L]^+$; 810.6, 100 $[CuL]K^+$; 794.6, 63 $[CuL]Na^+$ [L = $(Tr^{Mes,Me})^-$]. Anal. Calcd for $[C_{36}H_{43}N_9S_6BCu]_2$ (M_r = 1544.68): C, 55.98; H, 5.61; N, 16.32. Found: C 55.43; H 5.94; N 15.93. Colorless crystals suitable for X-ray structure determination were obtained from an acetonitrile solution, corresponding to $[Cu(Tr^{Mes,Me})]_2 \cdot 4CH_3CN$ (**4a**).

Preparation of $[Cu(Tr^{Me,o-Py})]_2$ (5). $[Cu(MeCN)_4]BF_4$ (0.109 g, 0.346 mmol) was added to a stirred suspension of $LiTr^{Me,o-Py}$ (0.204 g, 0.344 mmol) in methanol (30 mL). The mixture instantly became yellow. After 1 h the yellow solid was filtered off, washed with methanol (3 mL), vacuum-dried, and collected (0.181 g, 0.139 mmol, 81%). IR (KBr pellet, cm^{-1}): 3306 m, 3274 s, 3207 s, 2962 w, 2443 w br [ν(BH)], 1652 m, 1639 m, 1622 m, 1477 s, 1411 s, 1350 s, 1142 s, 1078 s, 1014 s. ^1H NMR (300 MHz, 270 K, $CDCl_3$; see discussion for signals attribution; the integration of the signals is reported separately for each isomer): δ 4.06 (s, 18H, CH_3 triazoline, e), 4.11 (s, 18H, CH_3 triazoline, e′), 7.30 (m, 6H/6H, CH py, b/b′), 7.64 (m, 6H, CH py, c), 7.74 (t, J = 6.6 Hz, 6H, CH

(26) Jochims, C. J. *Chem. Ber*. **1968**, *101*, 1746.
(27) Brunner, H.; Scheck, T. *Chem. Ber*. **1992**, *125*, 701−709.
(28) Gennari, M.; Giannetto, M.; Lanfranchi, M.; Marchiò, L.; Pellinghelli, M. A.; Tegoni, M. *Polyhedron* **2004**, *23*, 1829−1835.
(29) Leftin, J. H. *Chem. Abstr*. **1967**, *66*, 46487e.

Table 1. Summary of X-ray Crystallographic Data for **4a**, **5a**, and **6a**

	4a	**5a**	**6a**
empirical formula	$C_{80}H_{98}B_2Cu_2N_{22}S_6$	$C_{52}H_{48}B_2Cl_{12}Cu_2N_{24}S_6$	$C_{69}H_{80}B_2Cl_{10}Cu_2N_{18}S_4$
fw	1708.86	1775.60	1792.95
color, habit	colorless, block	colorless, block	colorless, block
cryst size, mm	0.25 × 0.08 × 0.08	0.45 × 0.35 × 0.20	0.30 × 0.20 × 0.15
cryst system	triclinic	triclinic	monoclinic
space group	$P\bar{1}$	$P\bar{1}$	$C2/c$
a, Å	11.130(1)	12.542(1)	31.568(9)
b, Å	13.395(2)	13.070(1)	13.690(3)
c, Å	14.998(2)	14.215(1)	21.026(7)
α, deg	92.233(3)	92.892(2)	90
β, deg	90.078(3)	115.559(1)	94.118(7)
γ, deg	94.367(2)	105.716(1)	90
V, Å^3	2227.8(5)	1985.6(3)	9063
Z	1	1	4
T, K	293(2)	293(2)	293(2)
ρ(calc), Mg/m^3	1.274	1.485	1.314
μ, mm^{-1}	0.672	1.148	0.904
θ range, deg	1.53−27.02	1.62−27.99	1.62−27.13
no. of rflcns/obsvns $F > 4\sigma(F)$	13 389/3378	21 694/5077	12 929/2891
R1[a]	0.0507	0.0525	0.0565
wR2[a]	0.0632	0.1212	0.0875

[a] $R1 = \Sigma||F_o| - |F_c||/\Sigma|F_o|$; $wR2 = [\Sigma[w(F_o^2 - F_c^2)^2]/\Sigma[w(F_o^2)^2]]^{1/2}$, $w = 1/[\sigma^2(F_o^2) + (aP)^2 + bP]$, where $P = [\max(F_o^2,0) + 2F_c^2]/3$.

py, c′), 7.93 (d, J = 7.5 Hz, 6H, CH py, d), 8.11 (d, J = 7.8 Hz, 6H, CH py, d′), 8.61 (m, 6H/6H CH py, a/a′). ^{13}C NMR (75 MHz, 298 K, $CDCl_3$): δ 33.96 (CH_3 triazoline), 124.06 (CH py), 124.18 (CH py), 124.45 (CH py), 136.63 (CH py), 148.54 (CH py), 167.74 (C═S), quaternary carbons not detected. Anal. Calcd for $[C_{24}H_{22}N_{12}S_3BCu]_2$ (M_r = 1298.13): C, 44.41; H, 3.42; N, 25.90. Found: C, 44.66; H, 3.49; N, 25.69. Colorless crystals suitable for X-ray structure determination were obtained from a chloroform solution, corresponding to $[Cu(Tr^{Me,o-Py})]_2 \cdot 4CHCl_3$ (**5a**).

Preparation of $[Cu(Br^{Mes,Me}pz^{o-Py})]_2$ (6). $[Cu(MeCN)_4]BF_4$ (0.092 g, 0.292 mmol) was added to a stirred suspension of $KBr^{Mes,Me}pz^{o-Py}$ (0.160 g, 0.242 mmol) in acetonitrile (50 mL). The mixture became bright yellow. After 2.5 h it was filtered, and the yellow solid was washed with acetonitrile (2 mL), vacuum-dried, and collected (90 mg, 0.066 mmol, 54%). IR (KBr pellet, cm^{-1}): 2966 w, 2920 w, 2859 w, 2497 w br [ν(BH)], 1597 w, 1578 w, 1489 m, 1433 m, 1414 s, 1369 m, 1327 m, 1204 m, 1114 m, 1092 m, 1033 m. ^{1}H NMR (300 MHz, 270 K, CD_2Cl_2; see discussion for signals attribution; the integration of the signals is reported separately for each isomer): δ 1.95 (s, 12H, CH_3 Mes, c, e), 2.00 (s, 12H, CH_3 triazoline, f), 2.02 (s, 12H, CH_3 Mes, c, e), 2.33 (s, 12H, CH_3 Mes, d), 6.75 (m br, 2H, CH m′), 6.81 (d, J = 2.1 Hz, 2H/2H, CH h/h′), 6.97 (s, 2H, CH Mes, a, b), 7.04 (s, 2H, CH Mes, a, b), 7.19 (m br, 2H/2H CH py, m/l′), 7.69 (m, J = 7.8 Hz, 2H/2H CH py, l/i′), 7.77 (d, J = 7.8 Hz, 2H CH py, i), 8.01 (s, br, 2H, CH py, n′), 8.35 (d, J = 4.2 Hz, 2H, CH py, n), 8.48 (s, br, 2H, CH pz, g′), 8.55 (d, J = 3.0 Hz, 2H CH pz, g). Some signals of the minor isomer (c′, d′, e′, f′, a′, b′) could not be detected as they are covered by the corresponding signals of the major isomer. Anal. Calcd for $[C_{32}H_{35}N_9S_2BCu]_2$ (M_r = 1366.00): C, 56.18; H, 5.16; N, 18.42. Found: C, 55.80; H, 4.92; N, 17.98. Yellow crystals suitable for X-ray structure determination were obtained from a dichloromethane solution, corresponding to $[Cu(Br^{Mes,Me}pz^{o-Py})]_2 \cdot 5CH_2Cl_2$ (**6a**).

X-ray Crystallography. The X-ray structure analysis on single crystals for the compounds $[Cu(Tr^{Mes,Me})]_2 \cdot 4CH_3CN$ (**4a**), $[Cu(Tr^{Me,o-Py})]_2 \cdot 4CHCl_3$ (**5a**), and $[Cu(Br^{Mes,Me}pz^{o-Py})]_2 \cdot 5CH_2Cl_2$ (**6a**) was performed on a Smart Bruker AXS 1000 area-detector diffractometer (Mo Kα = 0.710 73 Å). An absorption correction was applied using the program SADABS[30] with trasmission factors in the ranges 0.809−1.000 (**4a**), 0.696−1.000 (**5a**), and 0.907−1.000 (**6a**). The structures were solved by direct methods (SIR97[31]) and refined on F^2 with full-matrix least squares (SHELXL-97[32]), using the Wingx software package.[33] Non-hydrogen atoms were refined anisotropically, and the hydrogen atoms were placed at their calculated positions, except for the hydrogens of the B−H groups, which were found and refined. One of the two independent solvent molecules of crystallization ($CHCl_3$) in **5a** was found disordered in two positions with site occupancy factors of 0.8 and 0.2, respectively. For **6a**, four molecules of CH_2Cl_2/dinuclear complex were found, while the contribution of a fifth molecule was modeled with the program SQUEEZE PLATON.[34] The programs ORTEP3 for Windows[35] and Parst[36,37] were also used. X-ray data are reported in Table 1.

NMR Experiments. NMR spectra were recorded on a Bruker 300 MHz Avance spectrometer. Chemical shifts are reported in ppm, referred to residual solvent protons ($CDCl_3$, CD_2Cl_2, 1,1,2,2-tetrachloroethane-d_2, CD_3CN, DMSO-d_6). ^{13}C signals were assigned by means of (^{13}C−^{1}H)-HETCOR and DEPT (distortionless enhancement of polarization transfer) experiments. Two-dimensional experiments (HETCOR, COSY, and NOESY) were recorded using standard Bruker pulse sequences. Various 2D-NOESY experiments were recorded changing the mixing time (τ_m) in the range 0.2−0.8 s for **5** and **6**, and the best enhancement of the negative NOE peaks was obtained using a τ_m of 0.6 s. NOESY peaks intensities were determined by measuring peak volumes, and the distances between nuclei were determined according to the formula

$$r_{ij} = r_{ref}\left(\frac{V_{ref}}{V_{ij}}\right)^{1/6}$$

where V_{ij} and r_{ij} are the NOE cross-peak volume and the interproton

(30) *Area-Detector Absorption Correction*; Siemens Industrial Automation, Inc.: Madison, WI, 1996.
(31) Altomare, A.; Burla, M. C.; Camalli, M.; Cascarano, G. L.; Giacovazzo, C.; Guagliardi, A.; Moliterni, A. G. G.; Polidori, G.; Spagna, R. *J. Appl. Crystallogr.* **1999**, *32*, 115.
(32) Sheldrick, G. M. *SHELX97, Programs for Crystal Structure Analysis*, release 97-2; University of Göttingen: Göttingen, Germany, 1997.
(33) Farrugia, L. J. *J. Appl. Crystallogr.* **1999**, *32*, 837.
(34) Van der Sluis, P.; Spek, A. L. *Acta Crystallogr., Sect. A* **1990**, *46*, 194−201.
(35) Farrugia, L. J. *J. Appl. Crystallogr.* **1997**, *30*, 565.

distance of two protons *i* and *j* and V_{ref} is NOE cross-peak volume between two protons at a known distance r_{ref}. The distances between protons in compound **5** were determined by comparison between the H_d/H_c cross-peak intensity and the known $H_d\cdots H_c$ distance of 2.35 Å, whereas for compound **6** the distances between protons were determined by comparison between the H_g/H_h cross-peak intensity and the known $H_g\cdots H_h$ distance of 2.49 Å. Variable-temperature NMR experiments were recorded at 10 K intervals outside the coalescence regions and at 5 K intervals in proximity to the coalescence regions. These experiments were performed in the 210−350 K range ($CDCl_3$ as solvent) for **5** and in the 182−340 K range (CD_2Cl_2 as solvent) for **6** in controlled atmosphere valve NMR tubes. Free energies of activation (kJ/mol) for unequally populated sites[38] were calculated from the coalescence temperatures (T_c) and the frequency differences ($\delta\nu$) between the coalescing signals ($H_d/H_{d'}$ for **5** and $H_n/H_{n'}$ for **6**) extrapolated at the coalescence temperatures, using the formula

$$\Delta G_c^{\ddagger} = aT_c[9.972 + \log(T_c/\delta\nu)]$$

$$a = 1.914 \times 10^{-2}\ \text{kJ/mol}$$

Two- and one-dimensional FIDs were processed using the MestReC program suite.[39]

Quantum Chemical Calculations. All the calculations have been performed with the Gaussian 01 program suite.[40] Geometry optimization was performed for compounds **5** and **6** using initial coordinates derived from X-ray data (**5b** and **6b**) and on model geometries proposed on the basis of two- and one-dimensional NMR experiments (**5c** and **6c**). Since quantum mechanical studies on these dinuclear complexes were computationally demanding, we employed the two layers ONIOM technique also known as IMOMO.[41] The details about the ONIOM layers defined for the molecules in exam are reported in the Supporting Information. For the model system of **5** only the pyridine groups involved in the proposed fluxional process (one for each ligand) were retained on the triazoline rings whereas the remaining pyridine rings were approximated to hydrogen atoms. In the model system of compound **6** all the mesityl groups were approximated to hydrogen atoms and for both compounds the methyl groups on the triazoline rings were also approximated to hydrogen atoms. The gradient-corrected hybrid density functional B3LYP[42,43] and double-ζ basis set LANL2DZ with Hay and Wadt effective core potential (ECP)[44,45] were used for the description of the model system. Hartree−Fock with a minimum basis set LANL2MB with Hay and Wadt ECP were used for the "real system". For the geometry optimization of the model system, a polarization p-function for the hydrogen atoms of the B−H moiety and a polarization d-function for all sulfur atoms were added in the basis sets to give a better description of the interactions of these groups with the metals. Single point energy calculations were performed for all complexes using the B3LYP density functional and the LANL2DZ basis set.

Scheme 1

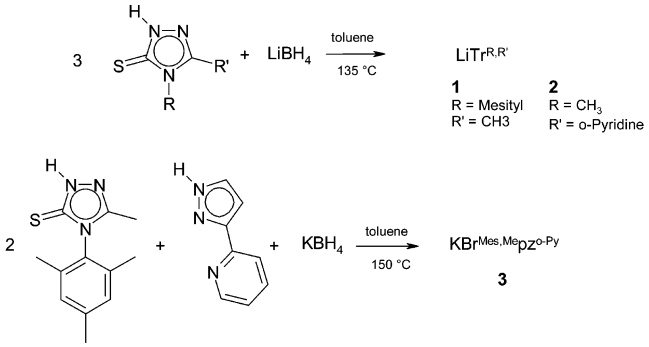

Electrochemistry. Cyclic voltammetry (CV) and differential pulse voltammetry (DPV) were performed in a three-electrode cell with a Pt disk as working electrode, a Pt rod as counter electrode, and a 0.1 M Ag/AgCl/KCl ($E^0 = +281$ mV) as reference electrode, by using a computerized electrochemical workstation consisting of an Autolab PGSTSAT 20 potentiostat (Ecochemie, Utrecht, The Netherlands) controlled by the GPES 4.9 software. Cyclic voltammograms were recorded on freshly prepared CH_2Cl_2 (**3** and **6**) or 1/1 CH_2Cl_2/CH_3CN (v/v) (**2**, **4**, and **5**) solutions containing 0.1 M supporting electrolyte [tetra-*n*-butylammonium hexafluorophosphate (TBAHFP) or tetra-*n*-butylammonium trifluoromethanesulfonate (TBAOTf)] and purged with N_2 for 2 min. All experiments were performed under identical conditions for different scan rates (50−1000 mV/s).

Results and Discussion

The synthesis of the tripodal ligand $LiTr^{Me,o-Py}$ (**1**)[28] and $LiTr^{Mes,Me}$ (**2**) were performed at high temperature in toluene by reacting triazoles and $LiBH_4$ in 3/1 ratio, Scheme 1. The method extensively employed to produce hydrotris(pyrazolyl)borate,[46] hydrotris(mercaptoimidazolyl)borate,[47] and hydrotris(thioxotriazolyl)borate,[48] which involves the reaction between borohydrides and heterocycles in the melt, could not be followed here due to the high and prohibitive melting temperatures of triazoles (>200 °C). Different strategies were attempted to synthesize the heteroleptic ligand **3**:

(36) Nardelli, M. *Comput. Chem.* **1983**, *7*, 95.
(37) Nardelli, M. *J. Appl. Crystallogr.* **1995**, *28*, 659.
(38) (a) Sandstrom, J. *Dynamic NMR Spectroscopy*; Academic Press: London, 1982. (b) Kost, D.; Carlson, E. H.; Raban, M. *Chem. Commun.* **1971**, 656−657. (c) Shanan-Atidi, H.; Bar-Eli, K. H. *J. Phys. Chem.* **1970**, *74*, 961−963.
(39) Cobas, J. C.; Sardina, F. J. Nuclear magnetic resonance data processing. MestRe-C: A software package for desktop computers. *Concepts Magn. Reson.* **2003**, *19A*, 80−96.
(40) Frisch, M. J.; Trucks, G. W.; Schlegel, H. B.; Scuseria, G. E.; Robb, M. A.; Cheeseman, J. R.; Zakrzewski, V. G.; Montgomery, J. A., Jr.; Kudin, K. N.; Burant, J. C.; Millam, J. M.; Stratmann, R. E.; Tomasi, J.; Barone, V.; Mennucci, B.; Cossi, M.; Scalmani, G.; Rega, N.; Iyengar, S.; Petersson, G. A.; Ehara, M.; Toyota, K.; Nakatsuji, H.; Adamo, C.; Jaramillo, J.; Cammi, R.; Pomelli, C.; Ochterski, J.; Ayala, P. Y.; Morokuma, K.; Salvador, P.; Dannenberg, J. J.; Dapprich, S.; Daniels, A. D.; Strain, M. C.; Farkas, O.; Malick, D. K.; Rabuck, A. D.; Raghavachari, K.; Foresman, J. B.; Ortiz, J. V.; Cui, Q.; Baboul, A. G.; Clifford, S.; Cioslowski, J.; Stefanov, B. B.; Liu, G.; Liashenko, A.; Piskorz, P.; Komaromi, I.; Gomperts, R.; Martin, R. L.; Fox, D. J.; Keith, T.; Al-Laham, M. A.; Peng, C. A.; Nanayakkara, A.; Challacombe, M.; Gill, P. M. W.; Johnson, B.; Chen, W.; Wong, M. W.; Andres, J. L.; Gonzalez, C.; Head-Gordon, M.; Replogle, E. S.; Pople, J. A. *Gaussian 01, Development Version*, revision B.01; Gaussian, Inc.: Pittsburgh, PA, 2001.
(41) (a) Humbel, S.; Sieber, S.; Morokuma, K. *J. Chem. Phys.* **1996**, *105*, 1959−1967. (b) Svensson, M.; Humbel, S.; Froese, R. D. J.; Matsubara, T.; Sieber, S.; Morokuma, K. *J. Phys. Chem.* **1996**, *100*, 19357−19363. (c) Dapprich, S.; Komaromi, I.; Byun, K. S.; Morokuma, K.; Frisch, M. J. *J. Mol. Struct. (THEOCHEM)* **1999**, *461−462*, 1−21.
(42) Becke, A. D. *Phys. Rev.* A **1988**, *38*, 3098.
(43) Becke, A. D. *J. Chem. Phys.* **1993**, *98*, 5648.
(44) Hay, P. J.; Wadt, W. R. *J. Chem. Phys.* **1985**, *82*, 299.
(45) Wadt, W. R.; Hay, P. J. *J. Chem. Phys.* **1985**, *82*, 284.
(46) Trofimenko, S. *Inorg. Synth.* **1970**, *12*, 99. Trofimenko, S. *Chem. Rev.* **1993**, *93*, 943−980.
(47) Reglinski, J.; Garner, M.; Cassidy, I. D.; Slavin, P. A.; Spicer, M. D.; Armstrong, D. R. *J. Chem. Soc., Dalton Trans.* **1999**, 2119−2126.
(48) Bailey, P. J.; Lanfranchi, M.; Marchiò, L.; Parsone, S. *Inorg. Chem.* **2001**, *40*, 5030−5035.

Scheme 2

$$2Li(Tr^{Mes,Me}) + 2Cu(CH_3CN)_4BF_4 \xrightarrow{MeOH,\ N_2} [Cu(Tr^{Mes,Me})]_2\ (\mathbf{4})$$

$$2Li(Tr^{Me,o\text{-}Py}) + 2Cu(CH_3CN)_4BF_4 \xrightarrow{MeOH,\ N_2} [Cu(Tr^{Me,o\text{-}Py})]_2\ (\mathbf{5})$$

$$2K(Br^{Mes,Me}pz^{o\text{-}Py}) + 2Cu(CH_3CN)_4BF_4 \xrightarrow{MeCN,\ N_2} [Cu(Br^{Mes,Me}pz^{o\text{-}Py})]_2\ (\mathbf{6})$$

(1) A step procedure was used that gives the hydrobis(thioxotriazolyl)borato first and the final product in a second phase from a reaction with 3-(2-pyridyl)pyrazole, which is analogous with similar synthesis reported in the literature.[49,50] This procedure gave no results as (a) reacting 4-mesityl-3-methyl-5-thioxotriazole with $LiBH_4$ or $NaBH_4$ in 2/1 ratio in THF at reflux condition gave a mixture of products together with unreacted reagents and (b) reacting 4-mesityl-3-methyl-5-thioxotriazole with $LiBH_4$ in 2/1 ratio (toluene, 50 °C) gave hydrobis(thioxotriazolyl)borato in good yield but the scarce solubility of this product in toluene even at high temperatures did not allow it to react with 1 equiv of 3-(2-pyridyl)pyrazole.

(2) The successful synthesis of **3** was obtained by a one-pot reaction between KBH_4, 3-(2-pyridyl)pyrazole, and 4-mesityl-3-methyl-5-thioxotriazole in 1/1/2 ratio (toluene, 150 °C), according to a modification of a reported method (Scheme 1).[51]

1−**3** are air-stable white solids. The neutral Cu(I) complexes were prepared at room temperature by reacting $[Cu(MeCN)_4]BF_4$ with **1**−**3** (Scheme 2). The stability of the ligands and of the resulting complexes in methanol allowed the synthesis in this solvent for **4** and **5**.

Crystal Structures. The Ortep diagrams of the three complexes are reported in Figures 1−3, and selected bond lengths and angles, in Tables 2−4. The coordination geometry of the metal for **4a** and **5a** are almost equivalent, with each copper(I) bound by three sulfur atoms in a distorted trigonal planar geometry. The complexes are dinuclear, and each ligand is *S*,*S* chelated on a metal center and bridges with the third sulfur atom a second metal. The Cu−S distances are in the range 2.253(1)−2.355(1) Å for **4a** and 2.252(1)−2.305(1) Å for **5a**. The distortion of the coordination geometry is evident from the analysis of the coordination bond angles: for **4a** they vary from 97.57(4) to 143.04(5)° whereas for **5a** they vary in a more narrow range from 111.54(4) to 124.63(4)°. The presence of a [B−H···Cu] interaction for both compounds is responsible for a distortion of the trigonal geometry toward the tetrahedral one. In fact, the Cu−H separation is of 1.99(3) Å (**4a**) and 1.94(4) Å (**5a**) and the metal lies out of the plane defined by the three sulfur atoms of 0.1138(5) Å for **4a** and 0.2237(5) Å for **5a** and is directed toward the B−*H* group. This type of molecular structure has been already reported for the dinuclear complex $[Cu(Tr^{Et,Me})]_2$ in which the peripheral part of the ligand (ethyl and methyl groups) provides a limited steric hindrance.[52] From a comparison of these molecular structures, it may be inferred that when these ligands are S_3H bound with an inverted geometry (with the B−H pointing toward the metal as in the reported molecular structures) the substituents on the triazoline rings play a minor role in determining the coordination geometry. It should be noted, however, that, in **4a**, the mesityl groups are blocked in a rigid position (perpendicular to the triazoline ring) to minimize the steric repulsion between the *ortho* methyl groups on the mesityl ring and the C=S and methyl group on the triazoline ring. This may limit the steric constraints that the mesithyl group may impose over the coordination geometry. As far as **5a** is concerned, the pyridine rings are pointing away from the coordination environment and therefore they are not directly influencing the copper(I) coordination. The distance between the two copper centers is 5.401(1) Å for **4a** and 5.308(1) Å for **5a** ruling out any metal−metal interaction.

A relevant difference with respect to the previously described molecular structures is exhibited by **6a** as the third "arm" of the heteroscorpionate ligand is represented by a *N*,*N* chelating pyrazolyl-2-pyridyl group. In the dinuclear complex each metal is in a trigonal geometry distorted toward the tetrahedral one and with the apical position occupied by the pyridine nitrogen atom. The overall coordination around copper may be described as S_2N,N' with each ligand *S*,*S* chelating on a metal center and bridging with the pyrazolyl nitrogen atom to a second metal. The copper atoms lie out of the *S*,*S*,*N* trigonal plane of 0.0672(6) Å, and they are directed toward the pyridine nitrogen atoms. Consequently, for this compound there is no evidence of a [B−H···Cu] interaction as the H···Cu separation is 2.83(3) Å and the B−H distance (0.97(3) Å) is significantly shorter than those found in compounds **4a** and **5a**. However, the $Cu-N_{pyridine}$ distance of 2.547(4) Å is consistent with a weak coordinative interaction. The distance between the two metals is 4.862(1) Å, and even though it is shorter than in **4a** and **5a**, it does not indicate a metal−metal interaction.

Solution Structures. The ^1H NMR spectrum of **4** in the temperature range 220−310 K in $CDCl_3$ (Supporting Information) is characterized by a single set of sharp signals

(49) Kimblin, C.; Hascall, T.; Parkin, G. *Inorg. Chem.* **1997**, *36*, 5680−5681.
(50) Alvarez, H. M.; Tran, T. B.; Richter, M. A.; Alyounes, D. M.; Rabinovich, D.; Tanski, J. M.; Krawiec, M. *Inorg. Chem.* **2003**, *42*, 2146−2156.
(51) Shu, M.; Walz, R.; Wu, B.; Seebacher, J.; Vahrenkamp, H. *Eur. J. Inorg. Chem.* **2003**, 2502−2511.
(52) Careri, M.; Elviri, L.; Lanfranchi, M.; Marchio, L.; Mora, C.; Pellinghelli, M. A. *Inorg. Chem.* **2003**, *42*, 2109−2144.

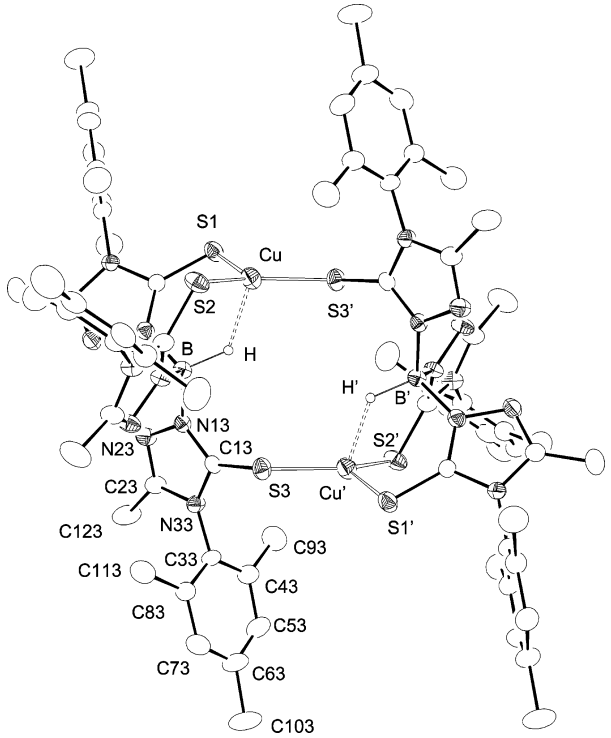

Figure 1. ORTEP drawing of **4a** at the 30% thermal ellipsoids level. Hydrogen atoms, except those of the B−H groups, have been removed for clarity.

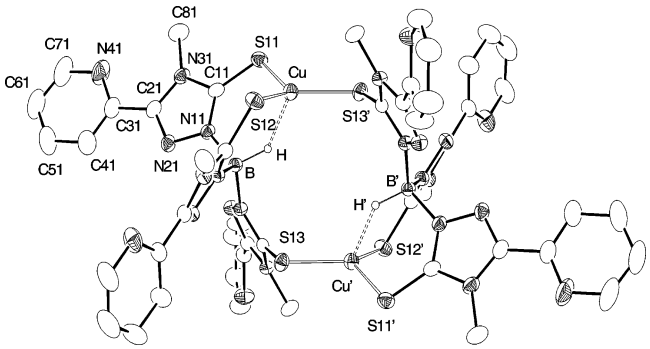

Figure 2. ORTEP drawing of **5a** at the 30% thermal ellipsoids level. Hydrogen atoms, except those of the B−H groups, have been removed for clarity.

despite the presence in the crystal structure of three distinct environments (corresponding to the three arms of each ligand) for both ligands in the dinuclear complex. The equivalence of the ligand arms observed in the NMR spectrum may result from a rapid interconversion of the triazolyl environments due either to a fast mononuclear−dinuclear equilibrium or to a fluxional process involving only the dinuclear complex. ^{1}H NMR at different concentrations (10^{-2}−10^{-4} M based on the dinuclear complex) show that the chemical shifts are concentration independent, and this would support a fluxional dinuclear complex hypothesis.

A different situation is encountered upon dissolution of crystals of **5a** and **6a** in various deuterated solvents ($CDCl_3$, CD_2Cl_2, 1,1,2,2-tetrachloroethane-d_2), as their ^{1}H NMR spectra show the presence of two species, Figures 4 and 5. The assignment of the peaks for every isomer for **5** and **6** was made by means of 2D-HETCOR (^{1}H−^{13}C) and 2D-COSY NMR spectroscopy (Supporting Information). As far

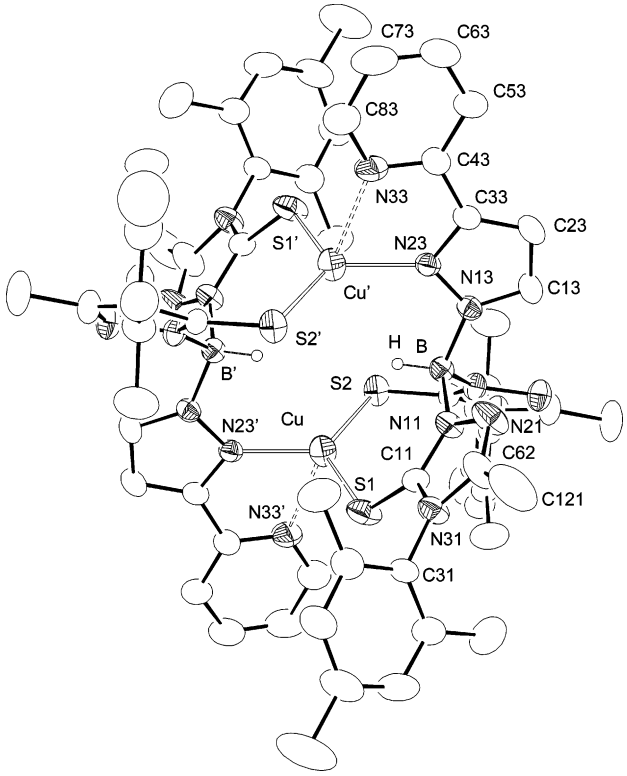

Figure 3. ORTEP drawing of **6a** at the 30% thermal ellipsoids level. Hydrogen atoms, except those of the B−H groups, have been removed for clarity.

Table 2. Experimental Selected Bond Lengths (Å) and Angles (deg) with Esd's in Parentheses for **4a**[a]

Cu−S(1)	2.355(1)	C(13)−S(3)	1.697(4)
Cu−S(2)	2.265(1)	B−H	1.27(3)
Cu−S(3)′	2.253(1)	B−N(11)	1.546(5)
Cu−H	1.99(3)	B−N(12)	1.539(5)
C(11)−S(1)	1.687(4)	B−N(13)	1.541(5)
C(12)−S(2)	1.694(4)		
S(1)−Cu−S(2)	118.56(4)	N(11)−B−N(12)	107.5(1)
S(1)−Cu−S(3)′	97.57(4)	N(11)−B−N(13)	111.3(3)
S(2)−Cu−S(3)′	143.04(5)	N(12)−B−N(13)	108.0(3)
S(1)−Cu−H	84.1(7)	N(11)−B−H	110(1)
S(2)−Cu−H	91.8(8)	N(12)−B−H	108(1)
S(3)′−Cu−H	100.0(7)	N(13)−B−H	113(1)
B−H−Cu	130(2)		

[a] Equivalent position: ′ = 1 − *x*, 1 − *y*, 2 − *z*.

as **5** is concerned, variable-temperature NMR experiments were performed in the range 350−210 K in $CDCl_3$. At 270 K two isomers are clearly distinguishable in the ratio major isomer/minor isomer of ∼2. Increasing the temperature leads to the coalescence of their signals, and above 335 K a single set of frequencies is observed. Furthermore, upon a decrease of the temperature below 220 K there is no substantial variation of the signals of the major isomer whereas, for the minor isomer, coalescence of its peaks occurs at 230 K and below this temperature three different environments can be observed. This confirms the presence of two equilibria, one involving the major and minor isomers (T_c = 335 K) and the other concerning only the minor isomer (T_c = 230 K). Two hypotheses can be made to explain this behavior: (1) The major isomer corresponds to a species with a symmetric structure as in the case of a mononuclear complex with the ligand S_3 bound, a trigonal geometry around the metal, and

Table 3. Experimental and Calculated Selected Bond Lengths (Å) and Angles (deg) with Esd's in Parentheses for **5a**−**c**[a]

	X-ray (**5a**)	calcd (**5b**)	calcd (**5c**)		X-ray (**5a**)	calcd (**5b**)	calcd (**5c**)
Cu−S(11)	2.305(1)	2.411	2.462	C(12)−S(12)	1.698(3)	1.707	1.714
Cu−S(12)	2.285(1)	2.384	2.397	C(13)−S(13)	1.708(3)	1.713	1.677
Cu−S(13)′	2.252(1)	2.363		B−H	1.15(3)	1.205	1.197
Cu−H	1.94(4)	2.004	2.473	B−N(11)	1.536(4)	1.542	1.536
Cu−N(23)			2.126	B−N(12)	1.537(4)	1.537	1.555
Cu−N(43)′			2.200	B−N(13)	1.555(4)	1.557	1.560
C(11)−S(11)	1.700(3)	1.702	1.706				
S(11)−Cu−S(12)	120.95(4)	125.22	120.24	S(11)−Cu−N(43)′			103.55
S(11)−Cu−S(13)′	111.54(4)	106.69		S(12)−Cu−N(43)′			95.23
S(12)−Cu−S(13)′	124.64(4)	123.62		N(23)−Cu−N(43)′			77.27
S(11)−Cu−H	86.0(8)	84.39		S(11)−Cu−N(23)′			138.59
S(12)−Cu−H	90.1(9)	86.82		S(12)−Cu−N(23)′			100.61
S(13)′−Cu−H	110.5(9)	121.35		N(11)−B−H	109(1)	109.20	109.14
N(11)−B−N(12)	110.2(3)	110.35	108.08	N(12)−B−H	109(1)	108.59	108.95
N(11)−B−N(13)	110.1(2)	109.67	113.15	N(13)−B−H	108(2)	107.49	108.51
N(12)−B−N(13)	111.5(2)	111.45	108.94	B−H−Cu	136(2)	136.32	

[a] Equivalent position: $' = -x, -y, -z$.

Table 4. Experimental and Calculated Selected Bond Lengths (Å) and Angles (deg) with Esd's in Parentheses for **6a**−**c**[a]

	X-ray (**6a**)	calcd (**6b**)	calcd (**6c**)		X-ray (**6a**)	calcd (**6b**)	calcd (**6c**)
Cu−S(1)	2.268(2)	2.408	2.385	C(12)−S(2)	1.679(5)	1.704	1.706
Cu−S(2)	2.245(1)	2.440	2.400	B−H	0.97(3)	1.191	1.200
Cu−N(23)′	1.985(3)	2.070	2.022	B−N(11)	1.537(6)	1.556	1.556
Cu−N(33)′	2.547(4)	2.226		B−N(12)	1.538(6)	1.561	1.555
Cu−H	2.83(3)	2.730	2.416	B−N(13)	1.520(6)	1.547	1.537
C(11)−S(1)	1.686(4)	1.702	1.707				
S(1)−Cu−S(2)	120.95(4)	113.21	116.89	N(11)−B−N(12)	109.7(4)	109.25	109.19
S(1)−Cu−N(23)′	111.54(4)	119.42	116.00	N(11)−B−N(13)	109.7(4)	110.24	110.61
S(2)−Cu−N(23)′	124.64(4)	126.55	120.71	N(12)−B−N(13)	111.0(4)	108.35	110.07
S(1)−Cu−H	77.2(9)	76.38	76.37	N(11)−B−H	111(2)	108.94	108.44
S(2)−Cu−H	68.7(9)	84.86	84.87	N(12)−B−H	104(2)	110.11	109.26
N(23)′−Cu−H	124.2(9)	133.04	133.03	N(13)−B−H	111(2)	109.94	109.23
S(1)−Cu−N(33)′	102.6(1)	107.87		B−H−Cu	126(2)	122.24	126.65
S(2)−Cu−N(33)′	99.0(1)	93.09					
N(23)′−Cu−N(33)′	71.5(1)	78.69					

[a] Equivalent position: $' = -x + 1/2, -y + 1/2, -z + 1$.

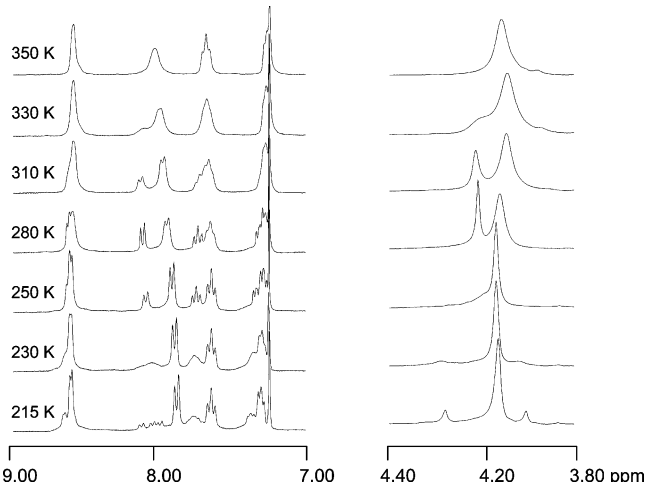

Figure 4. Temperature dependence of the ^{1}H NMR spectrum of **5** in $CDCl_3$: left, pyridine protons; right, methyl protons.

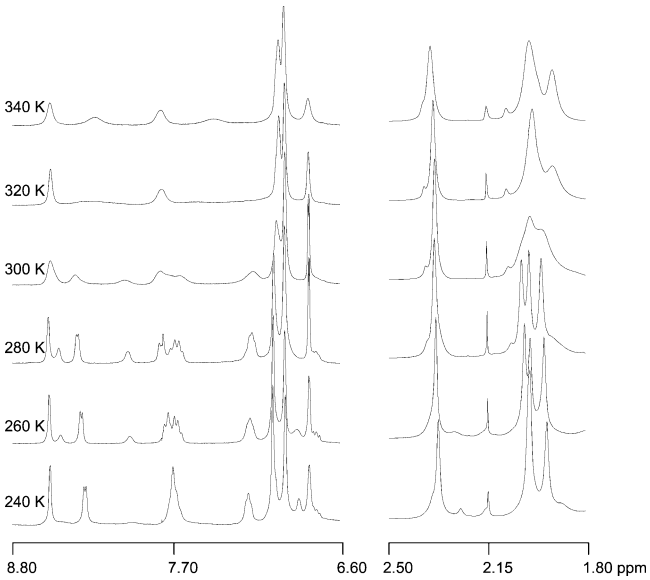

Figure 5. Temperature dependence of the ^{1}H NMR spectrum of **6** in CD_2Cl_2: left, aromatic protons; right, methyl protons.

a normal conformation of the ligand (with the B−H vector pointing outward). This could be possible thanks to the high flexibility of the ligand that chelates with eight-membered chelating rings and may be able to envelope the metal. The minor isomer presents a structure similar to the one reported in the solid state with nonequivalence between the three arms of the tripod, which becomes evident when decreasing the temperature below 230 K. (2) The major isomer corresponds to the structure reported in the solid state but with great stereochemical mobility that makes the three arms of the ligand equivalent in the temperature range under study, analogous with the behavior of compound **4**. The minor isomer is another dinuclear complex, the nonsymmetric

Scheme 3

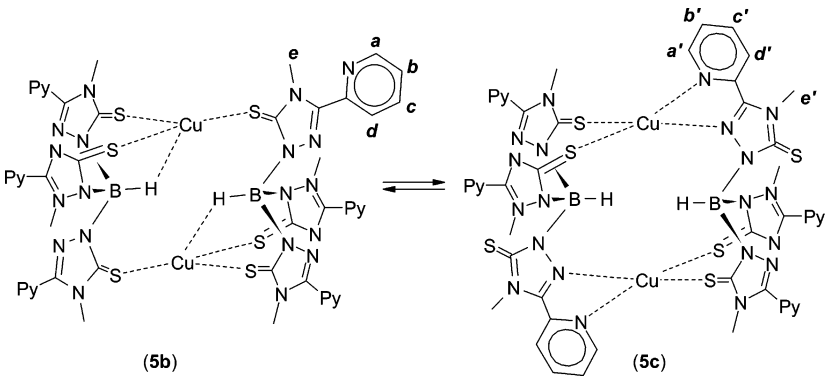

structure of which is evident below 230 K as three sets of signals appear. To distinguish between the two scenarios, mononuclear−dinuclear (1) or dinuclear−dinuclear (2) equilibria, ^{1}H NMR spectra were recorded at concentrations in the $10^{-2}-10^{-4}$ M range at 298 K (Supporting Information). These experiments show that the ratio of the integrals of the major and minor isomers is unvaried in this concentration range suggesting that the equilibrium with $T_c = 335$ K would involve two different dinuclear species (hypothesis 2) with an equilibrium constant of 0.5 for the formation of the minor isomer.[53] A possible structure of the minor isomer could involve the coordination of the ligand in a S_2N,N' mode so that it chelates *S,S* on a metal center and bridges on a second metal with the triazoline and pyridine nitrogen atoms deriving form the third arm. This would be in agreement with the observation that the signals in the pyridine region are at low fields compared to the corresponding signals of the major isomer, as a consequence of the involvement of the pyridine in the metal coordination. The resulting dinuclear structure would be centrosymmetric, but each ligand would present three different environments for each arm, giving rise to three sets of signals below 230 K. Increasing the temperature above this value may lead to the equivalence of the three arms of each ligand in accordance with the single set of frequencies observed in the NMR spectra. If this attribution is correct, the equilibrium with $T_c = 335$ K (between the two dinuclear complexes) would imply a rotation of the B−N bond for one arm of the ligand to replace the C═S group with the triazoline nitrogen atom in the copper coordination, Scheme 3. Moreover, if the pyridine is taking part in the metal coordination, it has to rotate of ∼150° around the $C_{triazoline}-C_{pyridine}$ bond according to the value of the torsion angle [N(2)−C(2)−C(3)−N(4)] of −150.3(4)° found for the solid-state structure.[54] Nevertheless, this would bring the $H_{d'}$ proton and the methyl ($H_{e'}$) on the triazoline ring in very close proximity, and this may represent a destabilizing factor for the structure of the minor isomer, Scheme 3. The proof that this *N,N′* chelation is possible comes from the structure of $[Ni(Tr^{Me,o-Py})_2]$ in which the ligand was in fact *S,N,N′* bound to the metal even though it adopted a normal conformation.[28]

(53) This value is obtained by the ratio of the integrals of the H_d and $H_{d'}$ protons (signals with no overlap).

(54) According to the X-ray structure of **5a** the pyridine rings are oriented in a way that places the nitrogen atom close to the methyl group of the triazoline ring and not on the same side of the triazoline nitrogen atom.

To help in the assignment of the molecular structures of the two isomers in solution, a 2D-NOESY NMR spectrum was recorded at 270 K in $CDCl_3$ (Supporting Information). At this temperature significant chemical exchange among the pyridine protons was evident from the positive cross-peaks in the NOESY spectrum. Intense negative cross-peaks are found for the protons of the same pyridine rings for the two conformers (separation of ∼2.3 Å). More interestingly, a weak cross-peak is found between the methyl protons and the H_a proton for the major isomer that correspond to an interproton distance of 3.74 Å, in good agreement with the equivalent separation found in the solid-state structure (mean value = 3.80(3) Å), Figure 6. This would confirm that for the major isomer the pyridine ring is oriented as in the solid-state structure (with the pyridine nitrogen facing the methyl group). For the minor isomer, the absence of a strong cross-peak between the methyl protons ($H_{e'}$) and the $H_{d'}$ proton could derive from a competition between the tendency of the pyridine to coordinate the copper center and the repulsion that would consequently arise between $H_{d'}$ and the methyl group. This would result in a structure in which the pyridine is nearly perpendicular to the triazoline plane exhibiting an incipient coordination to the metal. The free energy of activation derived from the coalescence temperature ($\Delta G^{\ddagger}_{335}$) for the process going from the major isomer to the minor

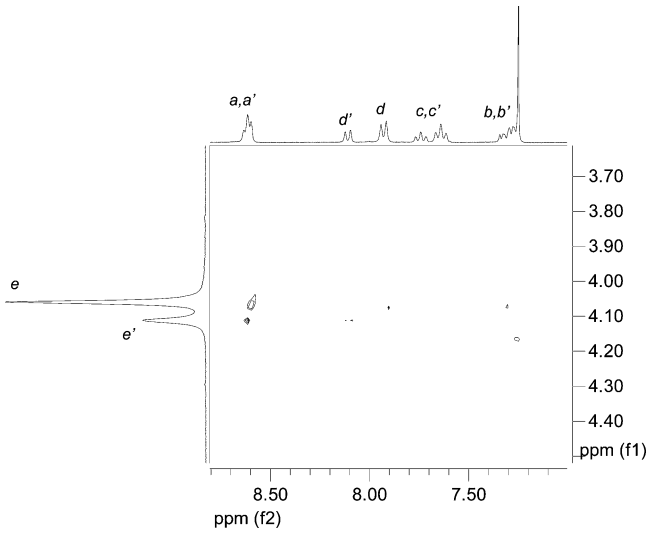

Figure 6. Aromatic and methyl regions of the NOESY NMR spectrum of **5** at 270 K in $CDCl_3$. Solid lines denote negative cross-peaks. See Scheme 3 for signal attribution.

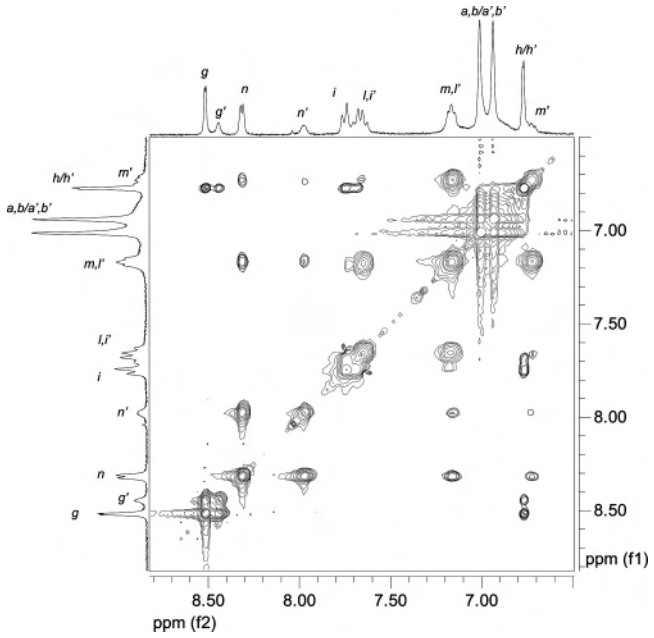

Figure 7. Aromatic region of the NOESY NMR spectrum of **6** at 270 K in CD_2Cl_2. Solid lines denote negative cross-peaks; dashed lines denote positive cross-peaks. See Scheme 4 for signal attribution.

isomer is 70.0 kJ/mol, whereas for the reverse process is 68.0 kJ/mol, Scheme 3.

For compound **6**, variable-temperature NMR experiments were performed in the range 340−182 K in CD_2Cl_2. At 280 K two isomers are clearly distinguishable with the ratio major isomer/minor isomer of 1.67 and the coalescence of their signals is observed at 320 K. Furthermore, decreasing the temperature below 250 K leads to the progressive disappearance of the minor isomer. Again, the question were we facing a mononuclear−dinuclear or dinuclear−dinuclear equilibrium arose, and ^{1}H NMR spectra were recorded at concentrations in the 10^{-2}−10^{-4} M range at 280 K (Supporting Information). The concentration-independent integral ratio confirmed the presence of an equilibrium involving only two dinuclear species with an equilibrium constant of 0.6 for the formation of the minor isomer at 280 K. A 2D-NOESY spectrum was recorded at 270 K to assign molecular structures in solution, Figure 7. At this temperature, the exchange rate between the two isomers is not negligible and positive cross-peaks are in fact evident in the pyridine, mesityl, and methyl regions and are complementing the 2D-COSY peaks attribution. Various negative cross-peaks are helpful in the assignment of the major isomer molecular structure. Strong negative cross-peaks are observed between the doublet centered at 6.81 ppm (H_h) and the multiplet centered at 7.75 ppm (H_i) and between the doublet at 8.32 ppm (H_n) and the singlet at 1.99 ppm ($H_{c/e}$) corresponding to an interproton distance of 2.46 and 2.62 Å, respectively. A cross-peak of intermediate intensity was also found for the multiplet centered at 7.66 ppm (H_l) and H_h.[55] These cross-peaks would confirm that in solution the molecular structure of the major isomer corresponds to the solid-state one. It is

(55) The interproton distances found in the solid-state structure are as follows: $D(H_h/H_i) = 2.50$ Å; $D(H_n/H_{c/e}) = 2.67$ Å.

Scheme 4

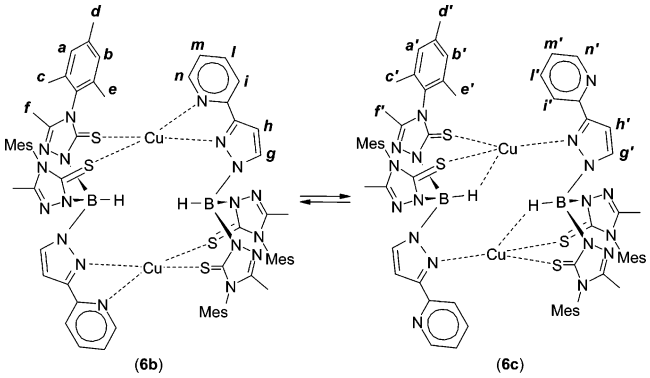

more difficult to extract information relative to the solution structure of the minor isomer as chemical exchange processes, affecting both positive and negative cross-peaks, hinder the interpretation. Moreover, decreasing the temperature to block the exchange processes leads to the disappearance of the minor species. According to the observation that the signals of the minor isomer in the aromatic region are at higher fields with respect to the corresponding proton signals of the major isomer, a molecular structure for the minor isomer can be proposed in which the pyridine is not coordinated to the metal. This can be achieved by a rotation along the $C_{pyridine}-C_{pyrazole}$ bond and by the approaching of the B−H moiety that pushes the pyridine nitrogen atom backward, Scheme 4. In this structure, the stabilization would come form the [B−H···Cu] interaction and by the disappearance of the H_i/H_h steric repulsion. In both molecular structures the ligand would present three distinct environments for each arm and a high fluxional behavior has to be considered to explain the single set of signals for each species in the 182−340 K temperature range. The $\Delta G^{\ddagger}_{320}$ for the process going from the major isomer to the minor isomer is 64.2 kJ/mol whereas for the reverse process it is 62.8 kJ/mol (Scheme 4).

DFT Calculations. To support the proposed fluxional processes evidenced by NMR spectroscopy for **5** and **6**, DFT geometry optimizations were performed starting from the geometry derived from the X-ray structural analysis (**5b**, **6b**) and on geometries proposed according to two-dimensional and variable-temperature NMR spectroscopy (**5c**, **6c**). The **b** structures correspond to the major isomers whereas the **c** structures correspond to the minor isomers as found in the NMR experiments. The drawings corresponding to the **5c** and **6c** optimized structures are reported in Figures 8 and 9, and the geometric parameters (bond distances and angles) for the optimized structures **5b,c** and **6b,c** are reported in Tables 3 and 4. The **5b** calculated structures agree very well with the experimental data obtained by X-ray diffraction. Nevertheless, an increase of the metal−S bond distances is exhibited probably due to the lack of the crystal packing forces present in the solid-state structures. In the **5c** structure the coordination at the metal may be described as S_2N,N' in which a C═S bridging group has been replaced by a bridging $N_{triazoline}-N_{pyridine}$ chelate system. Consequently, the H···Cu separation has increased to 2.437 Å diminishing the strength of the [B−H···Cu] interaction. The repulsive $(CH_3)_{triazoline}-$

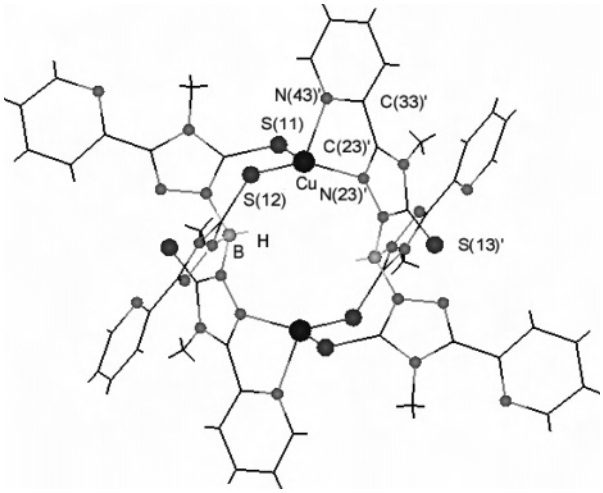

Figure 8. Optimized structure for the minor isomer **5c**.

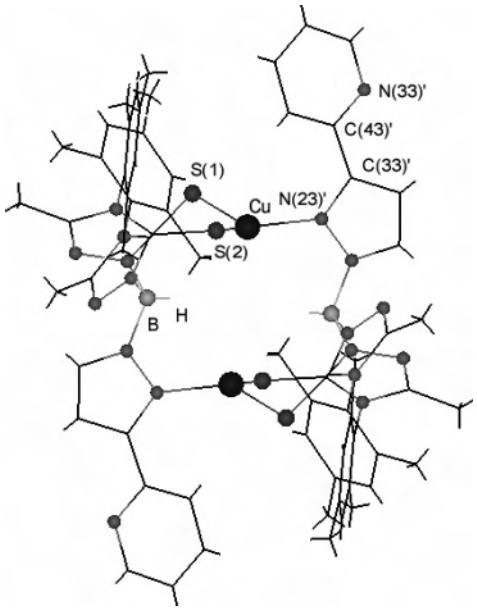

Figure 9. Optimized structure for the minor isomer **6c**.

$H_{d'}$ interaction that arises as a consequence of the *N*,*N*′ coordination is evidenced by the relatively high value of the torsion angle τ[N(23)−C(23)−C(33)−N(43)] of −18.8° (cf. 0° for an ideal conjugated and chelate aromatic system such as bipyridine). The corresponding torsion angles of sulfur bound ligand arms present absolute values of ∼160° in agreement with the values reported in the X-ray structure, and this may be a compromise between the stabilization that arises from the coplanarity/conjugation of the triazoline and pyridine rings and the repulsion between the $N_{pyridine}$ lone pair and the triazoline methyl group. With respect to the X-ray structure, the **6b** calculated structure shows an increase in the metal−S bond distances and only a slight elongation of the metal−$N_{pyrazole}$ one, whereas a more marked decrease (∼0.3 Å) for metal−$N_{pyridine}$ separation is observed. This would suggest a more pronounced interaction between the pyridine and Cu(I) if compared to the experimental structure. As a consequence of this interaction the torsion angle τ[N(23)−C(33)−C(43)−N(33)] is very small (1.7°). The H···Cu separation is ∼0.1 Å shorter than in the X-ray structure but still too large (2.730 Å) to account for a possible [B−H···Cu] interaction. For the **6c** calculated structure, the torsion angle τ[N(23)−C(33)−C(43)−N(33)] is 165.8° as a result of the pyridine ring rotation along the $C_{pyrazole}-C_{pyridine}$ bond with respect to **6b**. The H···Cu (2.416 Å) separation is ∼0.4 Å shorter than in the X-ray structure and ∼0.3 Å shorter than in **6b**, and this may be in agreement with a [B−H···Cu] interaction. This is also confirmed by the fact that the two metals in **6c** move away from the plane defined by the sulfur and nitrogen atoms and are directed toward the B−H groups. On the basis of these calculations, different copper(I) coordinations have been reported, namely S_3H, S_2N,N', S_2N,H, and it appears that the most stable coordinative environments are the S_3H (**4** and **5**) and S_2N,H (**6**) as may expected for a soft ion such as Cu(I).

The calculated energy difference (ΔE_{calc}) at the B3LYP/LANL2DZ level between the major and the minor isomers is 26.5 kJ/mol in **5** (ΔG_{335}(expt) = 2 kJ/mol) and 2.2 kJ/mol in **6** (ΔG_{320}(expt) = 1.4 kJ/mol). Whereas there is a good accordance between the experimental and calculated energy difference for the two isomers of **6**, compound **5** presents a more marked difference between the ΔG_{335} and the ΔE_{calc} values.[56] This poor agreement may be the result of (a) the level of calculation, which may not be accurate enough to give a ΔE_{calc} that reproduces the experimental value, and (b) the solvent effect, since the calculation are performed for an isolated system whereas the experimental ΔG_{Tc} are obtained in solution and the solvent can have a strong influence in stabilizing an isomer with respect to the other. In fact, for **5**, the ratio **5b**/**5c** is ∼8 in CD_2Cl_2, ∼2 in $CDCl_3$, and ∼0.7 in 1,1,2,2-tetrachloroethane-d_2.

Voltammetric Studies. The cyclic voltammograms of **4**−**6** are reported in Figure 10. Two main features appear from a comparison of the voltammograms of the three compound: (1) high anodic peak potential values (E_{pa}); (2) quasi-reversible behavior of the Cu(I)/Cu(II) couple.[57] The high E_{pa} values can be explained by considering the environment that surrounds the metal in the three compounds. In fact, with regard to the X-ray structures **4a** and **5a** three sulfur atoms are present in the copper coordination sphere along with a [B−H···Cu] interaction, whereas for **6a** two sulfur atoms and two nitrogen atoms represent the donor set. Even if one takes into account fluxional processes, at least two sulfur atoms are present in the coordination sphere of the metal, and this may be a factor that stabilizes Cu(I) with respect to oxidation.

The voltammogram of **4** shows an anodic peak at +719 mV correlated to a +538 mV cathodic one,[58] and they are assigned to the Cu(I)/Cu(II) couple, since its parent com-

(56) The energetics does not include zero-point energy or entropy corrections.

(57) Bard, A. J.; Faulkner, L. R. *Electrochemical Methods: Fundamentals and Applications*; John Wiley & Sons: New York, 1980.

(58) The correlation between the cathodic and anodic peaks has been performed by holding the potential at +800 mV for about 5 min. Restarting the scan in the cathodic direction resulted in an increase of the current of the correlated peak at +538 mV. The correlation between the anodic and cathodic peaks for compounds **5** and **6** has been performed in the same way by holding the potential at +0.700 and +0.500 mV, respectively.

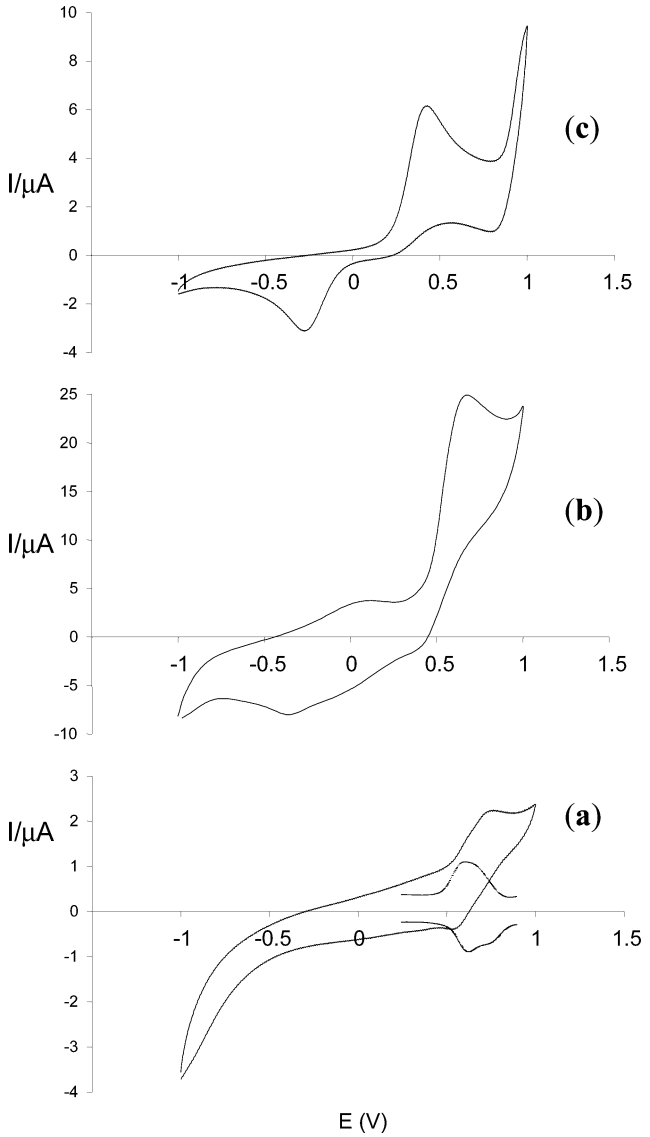

Figure 10. Cyclic voltammograms of (a) 10^{-4} M solutions of **4** dissolved in 1/1 CH_2Cl_2/CH_3CN (v/v) overimposed with the DPV scan (in the +0.25/+0.85 V window), (b) 10^{-3} M solutions of **5** dissolved in 1/1 CH_2Cl_2/CH_3CN (v/v), and (c) 10^{-3} M solutions of **6** dissolved in CH_2Cl_2. Supporting electrolyte: 0.1 M TBAHFP. Reference electrode: 0.1 M Ag/AgCl/KCl. Scan rate: 100 mV/s.

pound (**2**) shows two irreversible anodic peaks only at higher potentials (+960 and +1224 mV). The redox couple Cu(I)/Cu(II) is quasi-reversible, as shown by ΔE_p values (161 mV), implying a certain structural reorganization of the metal environment associated with the electron-transfer process. The scarce solubility of **4** in CH_2Cl_2/CH_3CN (1/1) (concentrated $\sim 10^{-4}$ M) resulted in a difficult detection of the electrochemical process, and to support the CV findings, a differential pulse voltammetry (that enhances the faradaic component of the signals) was performed on the same sample, which confirms the occurrence of the anodic and catodic events. Complex **5** shows rather different redox behavior. An anodic peak at +636 mV is correlated to a cathodic one at −316 mV, and they are assigned to the Cu(I)/Cu(II) couple. The quasi-reversibility of the procress (ΔE_p = 952 V) can be rationalized in terms of considerable coordination sphere modification resulting in copper(II) stabilization. This is in accordance with the fluxional behavior of the complex as evidenced by NMR spectroscopy since the proposed structure of the minor isomer implies the coordination of one arm of the ligand in the *N*,*N*′ fashion, a preferable coordinative situation for copper(II). The new species formed probably rearranges only a little in the following reduction; in fact, the subsequent anodic peak occurs at a lower potential (+123 mV) with respect to the initial species. This is confirmed by the fact that the occurrence of the anodic peak at +123 mV is particularly evident at the third scan of the potential in the anodic direction.

Complex **6** exhibits the anodic peak at +418 mV and the cathodic one at −319 mV attributable to the Cu(I)/Cu(II) couple, and the ΔE_p (+737 mV) is consistent with a quasi-reversible redox process. In the parent compound **3** two irreversible anodic events occur at higher potential (+770 and +1160 mV). Furthermore, a minor structural reorganization could be proposed for **6** if compared to **5** [ΔE_p(**5**) > ΔE_p(**6**)]. Also for this compound the electrochemical features could be explained according to its fluxional properties in agreement with the fact that, in **6**, only a weak-interacting pyridine nitrogen atom is displaced from the metal whereas, for **5**, the coordination environment is substantially different for the two species in equilibrium (S_3H and S_2N,N') requiring a greater reorganization energy. It has been reported that in some cases TBAHFP used as supporting electrolyte may interact with the species that undergo the electrochemical process and can alter their electrochemical behavior.[16] To confirm that this was not the case, the voltammograms were recorded in the same experimental conditions but using TBAOTf as supporting electrolyte without any appreciable changes to their redox features. This would support the hypothesis that the quasi-reversibility of the Cu(I)/Cu(II) redox couple is mainly due to ligand rearrangement contemporary with the electrochemical events.

Conclusions

Cu(I) complexes with homoscorpionate [$(Tr^{Mes,Me})^-$ and $(Tr^{Me,o-Py})^-$] and heteroscorpionate ligands [$(Br^{Mes,Me}pz^{o-Py})^-$] were synthesized. The X-ray characterization reveals that these compounds have a dinuclear structure in the solid state. The compounds $[Cu(Tr^{Mes,Me})]_2$ and $[Cu(Tr^{Me,o-Py})]_2$ exhibit equivalent coordination environment at copper (S_3H type supported by a [B−H···Cu] interaction). The ligand $(Tr^{Mes,Me})^-$ presents minor coordination capabilities (C═S groups) if compared to $(Tr^{Me,o-Py})^-$ for which an involvement of the *N*,*N*′ chelate system is also possible. Nevertheless, the similar solid-state structures for these compounds is in accordance with preference of Cu(I) for a sulfur-rich environment. This is also confirmed by DFT calculations, which suggest that the preferred Cu(I) environments in these systems are S_3H and S_2N,H. Nevertheless, the competition between the C═S and *N*,*N*′ systems for the Cu(I) coordination is evidenced by the solution fluxional behavior of $[Cu(Tr^{Me,o-Py})]_2$, as two species in equilibrium are present with a ratio that is also dependent on the deuterated solvents used. The proposed structure for the minor isomer of $[Cu(Tr^{Me,o-Py})]_2$ would

correspond to a species in which a C═S group has been replaced by a *N*,*N*′ system. This ligand flexibility (ability to display different donor sets) translates into nonreversible Cu(I)/Cu(II) redox processes due to stabilization of Cu(II) by involvement of N atoms for the metal coordination. Moreover, compounds $[Cu(Tr^{Mes,Me})]_2$ and $[Cu(Tr^{Me,o-Py})]_2$ exhibit high E_{pa} values due to Cu(I) stabilization by the soft ligand environment. From this point of view, an improvement of this situation has been achieved with the ligand $(Br^{Mes,Me}pz^{o-Py})^-$. In fact, in the coordination sphere of $[Cu(Br^{Mes,Me}pz^{o-Py})]_2$, the S_2N donor set is always present (even taking into account its fluxional behavior), and this grants a minor E_{pa} value for the couple Cu(I)/Cu(II) with respect to $[Cu(Tr^{Mes,Me})]_2$ and $[Cu(Tr^{Me,o-Py})]_2$. However, a direct comparison with $E°$ values of cupredoxins containing T1 copper sites is not possible as a consequence of the nonreversible properties of the Cu(I)/Cu(II) couple for the three compounds. Moreover, there is an additional question to be considered: in the blue copper protein the metal is forced into an energized state (entactic) by the protein framework that does not change conformation during the redox process. According to this theory, this protein rigidity at the active site is an essential requirement for the correct functioning of these proteins as electron carriers. Unfortunately, the model systems used in this work fail to satisfy this requirement, as they possess great stereochemical mobility. In fact, even though the geometry of the various isomers is essentially distorted tetrahedral as in cupredoxins T1 sites, the donor atom set changes from S_3H to S_2N,*N*′ in **5** and from S_2N,*N*′ to S_2N,*H* in **6** with the result that the redox processes are not reversible. With this respect we are currently investigating new Cu(I) model systems based on more conformationally rigid ligands that preserve the cupredoxins T1 center donor set.

Acknowledgment. This work was supported by the Ministero dell'Istruzione, dell'Università e Ricerca (Rome, Italy).

Supporting Information Available: Experimental details including preparation schemes, NMR spectroscpy, and X-ray crystallography (PDF). This material is available free of charge via the Internet at http://pubs.acs.org. Other supplementary crystallographic data for this paper are found in CCDC 256810−256812 (www.ccdc.cam.ac.uk/conts/retrieving.html).

IC048221J